Intrawell and interwell coupling of plasmons in multilayer modulation-doped $GaAs/Al_xGa_{1-x}As$ quantum wells

G. Fasol, R. D. King-Smith, D. Richards, and U. Ekenberg*
Cavendish Laboratory, Madingley Road, Cambridge CB3 0HE, England

N. Mestres† and K. Ploog
Max-Planck-Institut für Festkörperforschung, Heisenbergstrasse 1, D-7000 Stuttgart, West Germany
(Received 1 August 1988; revised manuscript received 6 February 1989)

Using electronic Raman scattering and calculations of the full random-phase-approximation inverse dielectric function, we show that in a modulation-doped $GaAs/Al_xGa_{1-x}As$ multiple-quantum-well structure with N quantum wells and M occupied subbands per well, the intrawell interactions split the plasmon dispersion into M groups of modes. The interwell Coulomb interactions split each group further into N eigenmodes and differ strongly between the different groups of plasmon modes. We observe "acoustic" plasmon modes in regions where Landau damping occurs. The splitting of the plasmon modes measures the strengths of the interwell and the intrawell interactions in modulation-doped $GaAS/Al_xGa_{1-x}As$ quantum wells. We determine the plasmon dispersion by electronic Raman scattering for a sample with three filled subbands per well and five superimposed wells. The present work shows how Raman scattering can be used to characterize multiple quantum wells with multiple subband occupations.

I. INTRODUCTION

Modulation-doped multiple quantum wells attract much interest because of their device applications (see, for example, Ref. 1) and because of their novel fundamental physical properties. Although plasmons in layered electron systems have been extensively studied theoretically,[2–6] there is a far smaller amount of experimental work[7–9] published, which can be used to test these calculations. Plasmons in layered electron systems have also been discussed in the context of high-temperature superconductivity in copper-oxide materials.[10] In this article we identify the hierarchy of effects of the interwell and of the intrawell interactions on the plasmon dispersion of an MBE-grown $GaAs/Al_xGa_{1-x}As$ multiple-quantum-well sample (where MBE means molecular-beam epitaxy) with several occupied subbands per well. In the course of this work we also observe and identify "acoustic" plasmon modes at low energies in the single-particle electron-hole continua, where Landau damping occurs. The aim of this article is twofold: It serves as a test of the accuracy of the large number of theoretical papers using the random-phase approximation (RPA) to investigate the properties of plasmons in layered electron systems, and second, it shows that the determination of the plasmon dispersion by electronic Raman scattering is a method to characterize complex multiple quantum wells with multiple occupation of the subbands as applicable for power (FET) field-effect transistor applications, for example.

In a single two-dimensional electron gas the plasmon dispersion depends as $q_{\parallel}^{1/2}$ on the in-plane wave vector $q_{\parallel}$.[11] In a modulation-doped quantum-well sample with N periods and a single occupied subband in each well, the plasmon branches of all sheets are coupled through the interwell Coulomb interaction and one finds a set of N intrasubband plasmons.[4,8,9] In the limit where N becomes infinite these modes form a continuous superlattice plasmon band whose dispersion relation is given within the RPA by the well-known expression[2,3,5]

$$\omega^2=\frac{2\pi n_s e^2 q_{\parallel}}{\epsilon m^*}\frac{\sinh(q_{\parallel}a)}{\cosh(q_{\parallel}a)-\cos(q_{\perp}a)}\ , \tag{1}$$

where $q_{\perp}$ is the wave-vector component perpendicular to the layer and all the other symbols have their usual meanings. In Eq. (1) the high-frequency, long-wavelength form of the RPA polarization propagator has been used. In addition it has been assumed that the electron sheets are infinitely thin. These two approximations are frequently used in calculations of the dielectric properties of layered electron systems—in the present paper we do not use these simplifying approximations: We use the *full* RPA dielectric function, we include the electronic-subband structure of our samples, and we use realistic electron wave functions calculated self-consistently to determine the plasmon dispersion.

A multiple-quantum-well structure with N wells and M occupied subbands per well has $N\times M$ plasmon eigenmodes. We show in the present work that the relatively strong intrawell interaction splits these plasmon modes into M groups. The N modes within each of these groups are split to varying degrees by the weaker interwell Coulomb interaction.

Using Raman spectroscopy, we measure the plasmon dispersion of a five-period multiple-quantum-well sample with three occupied subbands per well, except in the first well. We compute both the inverse dielectric response function and the density-density correlation function by

an extension of the results of King-Smith and Inkson.[5] This method is closely related to the formalism of Ref. 6. We take account of realistic electron wave functions determined by self-consistent calculations and of the population of several subbands within each well. We use the *full* expression for the random-phase-approximation polarizability (*full* means that we do not simplify the calculation by using the high-frequency long-wavelength approximation). Thus we can study the influence of Landau damping, which lies beyond the scope of the commonly applied high-frequency approximation. The influence of higher subbands on the plasmon dispersion of quantum wells was recently studied (see, for example, Refs. 3, 5, 12, and 13) and is also taken into account here.

II. EXPERIMENTAL DETAILS

The Raman measurements were performed using a krypton-ion laser pumped dye laser operating with LD700 dye, 0.85 m Spex double monochromator, and photon counting. The sample was situated in a helium-flow cryostat on a cold finger, which could be rotated around a vertical axis. There is no conservation of $q_\perp$ in the case of light scattering from a quantum-well sample with only five layers, since there is no translational symmetry perpendicular to the sample-growth direction.

Thus light coupling to all in-plane plasmons is possible—this is the effect which enabled us to see the splitting of the coupled-layer plasmons reported earlier.[9] We measure the layer plasmon dispersion as a function of $k_\parallel$ by varying the angle of the incoming- and the outgoing-light beam with respect to the plane of the quantum well and by accurately measuring the angle optically.[9]

The structure of the present sample is shown schematically in the insert of Fig. 1. Each of the five 500-Å-wide GaAs quantum wells is surrounded by a 50-Å AlAs spacer layer on the "inverted" side and by a 100-Å $Al_{0.3}Ga_{0.7}As$ spacer layer on the "normal" side, followed by a 250-Å-wide n-doped $Al_{0.3}Ga_{0.7}As$:Si layer. Note that the first well (next to the substrate) has a dopant layer on one side only and therefore contains approximately half as many carriers as the other wells of the system. This is taken into account in our calculation. The present sample has a mobility of 245 000 $cm^2/V\,s$ (determined by Hall measurements at 6 K after saturating illumination).

III. SAMPLE CHARACTERIZATION AND SELF-CONSISTENT BAND-STRUCTURE CALCULATIONS

In the course of this work we found similar results in 12 samples, and for the present paper we concentrate on one sample, which consists of five superimposed periods as described above. We have characterized this structure as follows.

(1) Figure 2 shows Raman scattering measurements of the intersubband excitations. In crossed polarization and in resonance with the $E_0+\Delta_0$ gap the single-particle intersubband excitations are seen. These spectra show in-

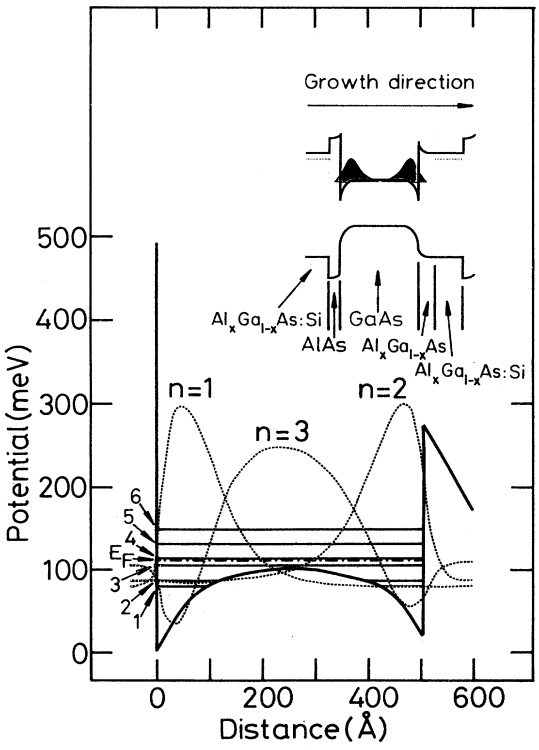

FIG. 1. Hartree potential and wave functions determined by self-consistent calculations for asymmetric quantum wells studied here.

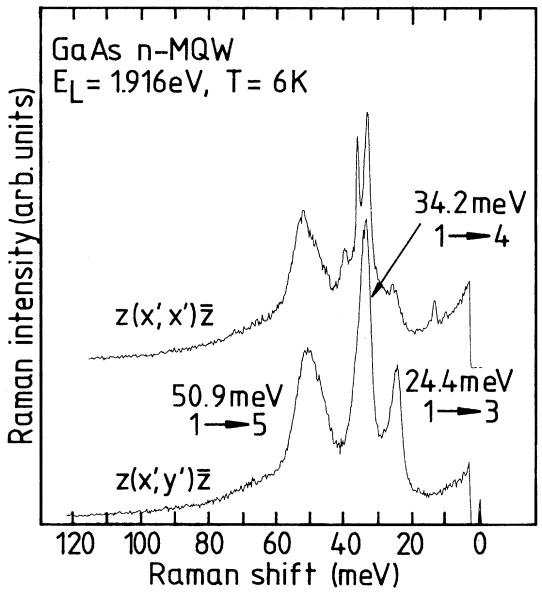

FIG. 2. Intersubband Raman spectra are used to determine the subband structure of the sample. The peaks in the single-particle spectrum measured in crossed polarization $z(x',y')z$ yield the intersubband spacings as indicated. Parallel polarization spectra $z(x',x')z$ yield the intersubband plasmon modes. MQW means multiple quantum well.

TABLE I. Calculated subband energies and subband occupations for the present sample. (Energies are measured from the potential minimum next to the "inverted" heterojunction).

	Subband energy (meV)		Subband occupation N_s (cm^{-2})	
Subband No.	Numerical integration	Variational[a] method	Numerical integration	Variational[a] method
1	79.8	81.1	9.0×10^{11}	8.7×10^{11}
2	85.5	86.5	7.2×10^{11}	7.4×10^{11}
3	104.3	106.4	1.8×10^{11}	1.8×10^{11}
4	114.0	115.9	0	0
5	132.5	130.7	0	0
6	149.9	152.4	0	0

[a]Reference 16.

tersubband transition energies of 24.4, 34.2, and 50.9 meV, respectively.

(2) Hall measurements at $T=6$ K, under saturating illumination and with a magnetic field of 1 kG yield a total carrier concentration of 5.4×10^{12} cm^{-2} and a mobility of $\mu=245\,000$ cm^2/V s.

(3) Raman measurements of the in-plane single-particle excitation spectra[9] are shown in Fig. 3. They are found to measure the carrier concentration at the high mobility, "normal" interface. Their fit[14] with the Lindhard-Mermin dielectric function determines a carrier density of 0.74×10^{12} cm^{-2} at the "normal" interface and a single-particle scattering time of $\tau_{sp}=1.5$ ps at $T=7.5$ K. [The small features at the higher-energy side of the main single-particle excitation peak are likely to be due to some penetration of the plasmon mode "Q" of Fig. 5(a)].

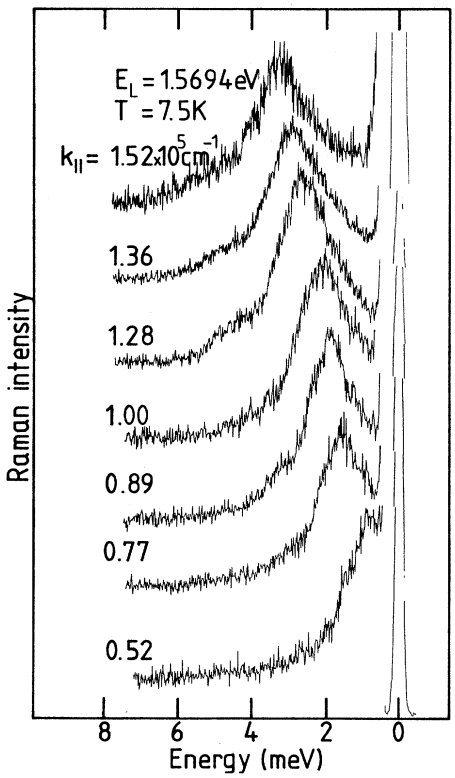

FIG. 3. Intrasubband single-particle Raman spectra. These spectra yield the carrier concentration at the "good" interface.

In addition, we have performed luminescence, luminescence excitation, and Shubnikov–de Haas measurements on several samples of the same series. Combining the various experimental results with self-consistent band-structure calculations, we build a consistent picture of the subband structure and the subband occupation densities.

We solve Poisson's equation and the effective-mass Schrödinger equation self-consistently using both numerical integration[15] and a variational method,[16] neglecting exchange and correlation contributions to the potential[17] to determine the subband structure and the wave functions. Both methods yield very similar results, as shown in Table I. Selfconsistency was achieved using the standard iteration method described in the review article of Ando, Fowler, and Stern.[15] For the band offsets we use[18] $\Delta E_c/\Delta E_{gap}=0.69$. We assume that the conduction subbands fill up until the Fermi level reaches the position of the donor levels outside the depletion regions. The transition energies between several of the lowest subbands are determined from intersubband Raman spectra measured in crossed polarization as shown in Fig. 2. By comparing these experimental subband separations with the calculated values we determine the subband energies and the population of the subbands as shown in Table I. The self-consistently calculated Hartree potential and wave functions are shown in Fig. 1. These results agree well with those of a variational calculation[16] using a modification of the methods of Ref. 19. The electrons in the lowest subband ($N=1$) are localized at the inverted interface, those for the second subband are localized at the normal interface. The charge density for the third level has a strong peak in the middle of the well and secondary maxima both at the inverted and at the normal interfaces. We attribute the difference in carrier distribution reported for a different sample[9] to the difficulty of obtaining the electron density localized at the inverted interface by Shubnikov–de Haas measurements alone since these electrons have low mobility.

IV. PLASMON DISPERSION

A. Measurements

Figures 4(a) and 4(b) show Raman spectra of the coupled-layer plasmon modes of the present sample as a

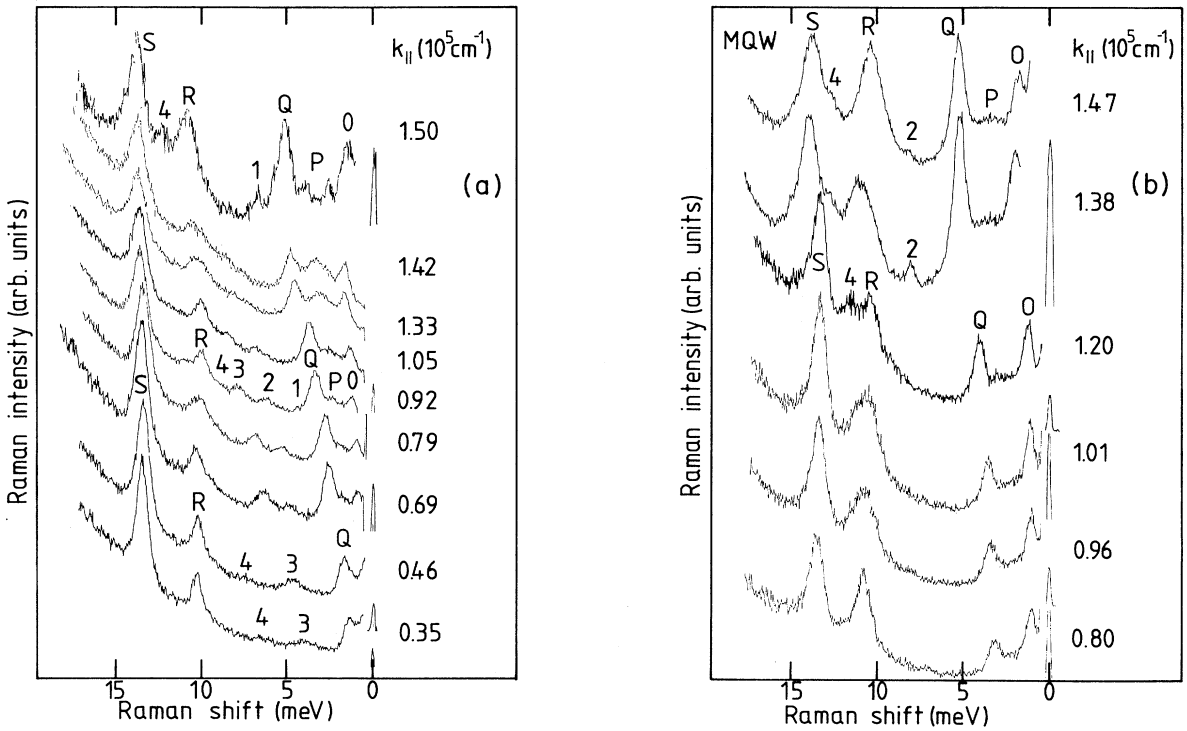

FIG. 4. Raman spectra of coupled-plasmon modes of modulation-doped quantum well with five periods, as a function of the in-plane wave-vector component $k_{\parallel}$. Letters (O,P,Q,R,S) and numbers (1,2,3,4) refer to the different types of plasmon modes discussed in the text. The temperature is $T=10$ K. (a) $E_{\text{laser}}=1.5566$ eV, (b) $E_{\text{laser}}=1.5616$ eV.

function of in-plane wave-vector component $k_{\parallel}$, measured with two different laser energies. The laser energies are in both cases close to the lowest excitation energy, so that these measurements are done close to the E_0 resonance. The dependence of these spectra on the laser energy shows the importance of resonance effects, which we are investigating at present. The spectra show a set of peaks (O,P,Q,1,2,3,4) which vary strongly as a function of $k_{\parallel}$. We attribute these peaks to coupled-layer intrasubband plasmon modes. A second set of Raman signals (R near 10.5 meV and S near 13.8 meV), depend only weakly on $k_{\parallel}$, and are therefore attributed to intersubband excitations. Peak S is assigned to the $3\rightarrow 4$ intersubband plasmon transition. Signal R could be due to an intersubband transition in the first quantum well grown next to the substrate, which has a dopant layer on one side only. Signal P could also be due to this well. An alternative explanation would be that P and R are due to lower carrier concentration in the quantum well next to the surface due to surface depletion. The $1\rightarrow 2$ collective intersubband transition is not observed, because the corresponding wave-function overlap is too small, as shown in Fig. 1.

Figure 5(a) shows the plasmon resonances of the sample as a function of $k_{\parallel}$. The shaded areas in Fig. 5(a) show the regions of both intrasubband and intersubband single-particle continua. Modes Q and 1, 2, 3, 4 are observed both outside and within the regions of intersubband Landau damping. In the bulk, plasmons would be strongly Landau damped within the regions of single-particle excitations. Our work shows that in a layered sample, the coupling of intrasubband collective modes to the single-particle excitations is weak.[9] We observe acoustic-type (i.e., linear dispersion) intrasubband plasmons in the region, where Landau damping, i.e., decay into intrasubband electron-hole excitations is possible. This is an important result, which confirms speculations about the nature of acoustic plasmon modes in superlattices.[12,20] This behavior is completely different from three-dimensional systems, where the plasmons become strongly damped, when their dispersion is in a region of Landau damping—they decay strongly into single-particle excitations.

The sample consists of five wells. In the present calculation, four of the wells have three filled subbands. For the well closest to the substrate, we use half the regular carrier concentration and take only two filled subbands. Thus there are 14 sheets of electrons in total and consequently we expect the complete intrasubband plasmon dispersion to consist of 14 branches. Because of the complexity of this situation, we proceed in two steps to explain the plasmon dispersion. First we study the plasmon dispersion of a single isolated well in a simple model, and second we calculate the density-density correlation function and the plasmon frequencies for the full five-well sample, using realistic wave functions from the self-consistent band-structure calculation. The plasmon eigenmodes are determined by calculating the real-space inverse dielectric function using the methods set out in Ref. 5.

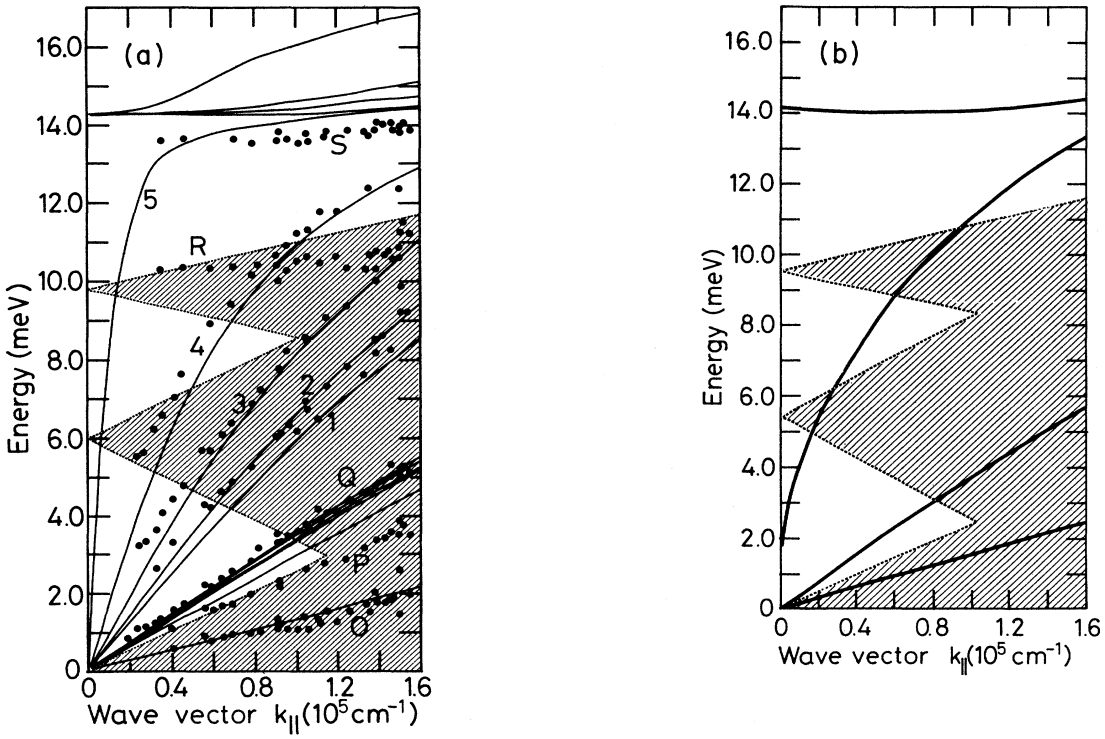

FIG. 5. (a) Experimental points and full RPA calculation (thin solid lines) of plasmon modes of a modulation-doped quantum well with five periods and three filled subbands per well. Regions of Landau damping are shaded. Intrawell interaction splits the modes into three groups: group O, group Q, and the group of modes 1,2,3,4,5. Each group of modes corresponds to a plasmon eigenmode of a corresponding single well, as shown in (b). Interwell interaction splits the modes within each of these groups into individual plasmon eigenmodes. Mode P is the asymmetric "acoustic" plasmon mode of the first well. Mode 5 mixes strongly with intersubband mode S. (b) Calculated plasmon dispersion for a *single* quantum well with the same subband structure and carrier densities as one single period of the sample, for which results are shown in (a). As there are three filled subbands in the quantum well, there are three coupled plasmon modes. In addition, one intersubband plasmon appears near 14.1 meV. The shaded areas show the intrasubband and the $1\rightarrow 2$ and $3\rightarrow 4$ single-particle excitation continua.

B. Calculations for a single well

At first we determine the plasmon dispersion of a single isolated quantum well in a simple model. We assume a well of width $2b$ with three filled subbands resembling a single-period of our multiple-quantum-well sample. We assume that the two lowest subbands have equal population $n_1=n_2$ and that their charge densities are located as infinitely thin layers at the "normal" and at the "inverted" interface of the well. The charge density n_3 populates the third subband and is located on an infinitely thin layer in the middle of the well. We assume further that $n_3 \ll n_1=n_2$, and we neglect interband scattering and image potentials. The plasmon dispersion is given by the solutions of

$$\mathrm{Det}\begin{vmatrix} 1-\frac{\omega_{11}^2}{\omega^2} & -\frac{\omega_{12}^2}{\omega^2} & -\frac{\omega_{13}^2}{\omega^2} \\ -\frac{\omega_{21}^2}{\omega^2} & 1-\frac{\omega_{22}^2}{\omega^2} & -\frac{\omega_{23}^2}{\omega^2} \\ -\frac{\omega_{31}^2}{\omega^2} & -\frac{\omega_{32}^2}{\omega^2} & 1-\frac{\omega_{33}^2}{\omega^2} \end{vmatrix}=0 , \tag{2}$$

$$\omega_{\mu\mu'}^2=\frac{2\pi n_s^{\mu} e^2 q_{\parallel}}{\epsilon m^*}\int\int A^{\mu}(z)e^{-q_{\parallel}|z-z'|}A^{\mu'}(z') \times dz\,dz' . \tag{3}$$

In Eq. (3) we are using the high-frequency form for the polarization propagator. Since we assume in the present section that the electrons are on infinitely thin sheets at the edges and in the middle of the well, the wave functions are $A^1(z)=\delta(z-b)$, $A^2(z)=\delta(z+b)$, and $A^3(z)=\delta(z)$.

We obtain the following plasma frequencies:

$$\omega_1^2=\frac{2\pi n_1 e^2 q_{\parallel}}{\epsilon m^*}(1+e^{-2q_{\parallel}b}) , \tag{4}$$

$$\omega_2^2=\frac{2\pi n_1 e^2 q_{\parallel}}{\epsilon m^*}(1-e^{-2q_{\parallel}b}) , \tag{5}$$

$$\omega_3^2=\frac{2\pi n_3 e^2 q_{\parallel}}{\epsilon m^*}\left[\frac{1-e^{-2q_{\parallel}b}}{1+e^{-2q_{\parallel}b}}\right] . \tag{6}$$

In the long-wavelength limit ($q_{\parallel}b \ll 1$) ω_1 is proportional to $q_{\parallel}^{1/2}$, while both ω_1 and ω_2 are proportional to $q_{\parallel}$,

representing acoustic plasmon modes. The dispersion of these plasmon modes is shown in Fig. 5(b) together with the $3\rightarrow4$ intersubband plasmon and the intrasubband, $1\rightarrow2$ and $3\rightarrow4$ intersubband single-particle continua. Comparing the plasmon dispersion of the single well [Fig. 5(b)] with that of the five-well sample [Fig. 5(a)], clearly shows how the interwell Coulomb interaction splits the plasmon bands.

The electrical potentials $\Phi_\nu(z)$ corresponding to these three plasmon modes are

$$\Phi_1(z)\propto e^{-q_\parallel|z-b|}+\frac{2e^{-q_\parallel b}n_3^2}{n_1^2(1+e^{-2q_\parallel b})}e^{-q_\parallel|z|}+e^{-q_\parallel|z+b|}, \tag{7}$$

$$\Phi_2(z)\propto e^{-q_\parallel|z-b|}-e^{-q_\parallel|z+b|}, \tag{8}$$

$$\Phi_3(z)\propto e^{-q_\parallel|z-b|}-(e^{-q_\parallel b}+e^{q_\parallel b})e^{-q_\parallel|z|}+e^{-q_\parallel|z+b|}. \tag{9}$$

These electrical potentials are demonstrated in Fig. 6. The potential Φ_1 for the highest-energy plasmon mode in Fig. 6(a) decays relatively slowly outside the well. The potential Φ_2 for the intermediate mode decays much more rapidly, while for the lowest energy mode the electrical potential Φ_3 vanishes outside the wells.

The carrier-density modulations parallel to the plane of the well are shown in Fig. 7(a) for the highest frequency mode ($\nu=1$) and in Fig. 7(b) for the mode $\nu=2$. The carrier-density modulations are shown for the carriers in the lowest subband ($n=1$) at the inverted interface, in the second subband ($n=2$) at the normal interface, and in the third subband ($n=3$) in the middle of the well.

Calculating the eigenvectors and the electric potentials $\Phi_\nu(z)$ corresponding to the three coupled plasmon modes, we find that for the highest frequency mode ($\nu=1$) all electrons move in phase, producing the highest possible field outside the well. For the mode $\nu=2$ the charges at both interfaces move antisymmetrically, whereas the charges in the middle of the well do not move appreciably. Thus the fields outside the well are smaller than for the plasmon move $\nu=1$. For the lowest energy mode ($\nu=3$) the fields outside the well are very small. Thus it is obvious that in a multiple quantum well, plasmons of type $\nu=1$ will show strong Coulomb coupling, plasmons of type $\nu=2$ will show much weaker coupling, and those of type $\nu=3$ cannot show any Coulomb coupling at all.

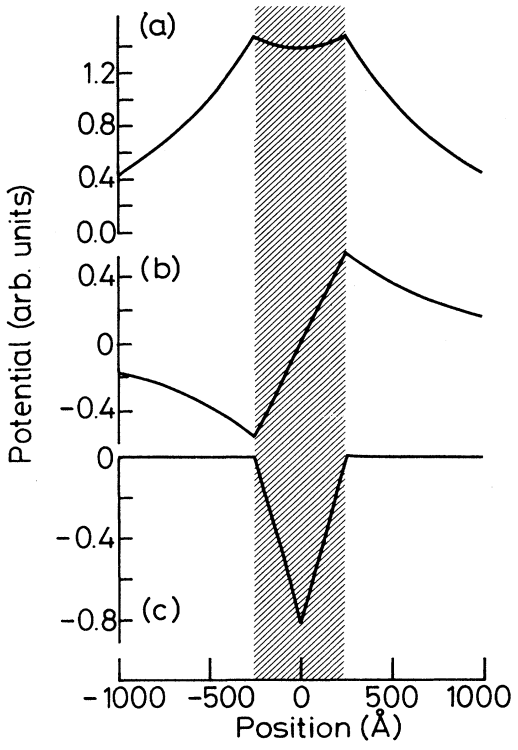

FIG. 6. Electrical potential associated with the three plasmon eigenmodes ω_1, ω_2, ω_3 of a single quantum well with three filled subbands using the model of Sec. IV B. The shaded area shows the thickness of the quantum well. (a) Highest energy mode ω_1, (b) intermediate mode ω_2, (c) lowest energy mode ω_3. Note that for the lowest energy mode ω_3, the carriers move such that the potential outside the well is zero. Thus there cannot be any Coulomb coupling between wells for mode ω_3.

C. Calculations for the five-well sample

If we bring several such single quantum wells together from infinite separation, the fivefold degenerate modes will interact due to the interwell Coulomb interaction and a set of nondegenerate plasmon modes will result. The stronger the interwell interaction, the stronger we expect the splitting to be. The strength of the interwell interaction for a particular type of mode will depend on the Coulomb field outside the wells. Thus the single-well mode $\nu=1$ at highest energy has maximum Coulomb field outside the well, and therefore the interwell

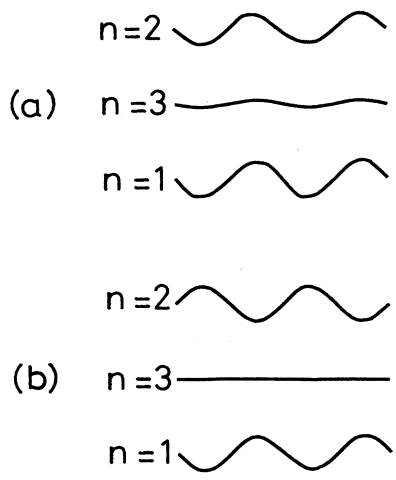

FIG. 7. Charge-density modulation parallel to the quantum well plane. (a) Highest energy mode ω_1, (b) intermediate mode ω_2. We do not show the result for the Landau damped lowest energy mode ω_3.

Coulomb coupling is expected to be maximal. Similarly, we expect the interwell Coulomb coupling to be intermediate for modes of type $\nu=2$ and negligible for modes of type $\nu=3$. The modes for $\nu=2$ and for $\nu=3$ are acoustic plasmon modes, and they are closely related to the plasmons studied in Ref. 12.

To demonstrate this behavior, we show the results of our full plasmon dispersion calculation as the solid lines in Fig. 5(a). We have now taken the realistic wave functions from our self-consistent band-structure calculation and the *full* RPA forms for the polarization propagators to include the effects of Landau damping within the electron-hole continua.[5,11] Outside the shaded Landau damping regions, we obtained the plasmon dispersion by searching for the zero's of the determinant of the dielectric function. Within the electron-hole continua, we obtain the plasmon spectra by calculating the imaginary part of the density-density correlation function $[\mathrm{Im}D(q_{\|},z,z,\omega)]$ which is directly related to the inverse dielectric response function. It has peaks at those frequencies, where long-lived Landau-damped plasmons exist, as shown in Figs. 8(b). The result shown is for

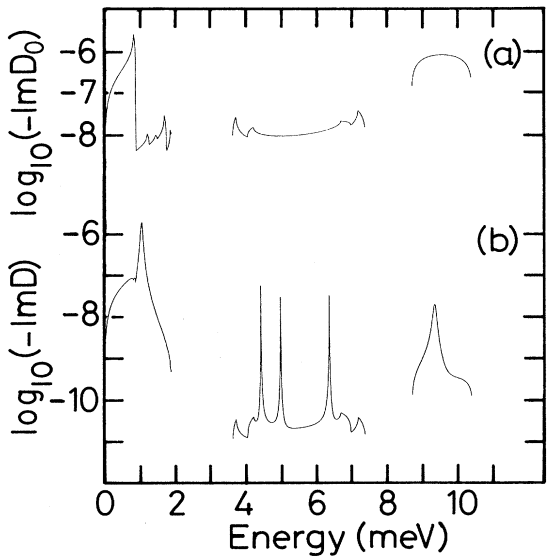

FIG. 8. Imaginary part of the density-density correlation function calculated for the present sample to demonstrate the character of the plasmon resonances within the regions of the single-particle excitation continua. (a) The imaginary part of the density-density correlation function D_0 for vanishing Coulomb interaction between electrons—the RPA polarizability. This case corresponds to the single-particle excitations. (b) $\mathrm{Im}(-D)$ including Coulomb interaction. The calculation is for $q_{\|}=0.7\times10^5$ cm^{-1}. Weakly Landau damped plasmon resonances within the single-particle continua appear as spikes near 1.1, 4.4, 5.0, 6.3, and near 9.3 meV. The single-particle intrasubband continua are visible as the background below 2.0 meV, the continuum of the $1\rightarrow2$ intersubband single-particle excitations is visible as the background between 3.6 and 7.5 meV. Between 8.6 and 10.3 meV, the $3\rightarrow4$ intersubband single-particle continuum is visible.

$q_{\|}=0.7\times10^5$ cm^{-1}. It can be seen that there are a series of sharp spikes at energies of about 1.1, 4.4, 5.0, 6.3, and 9.3 meV. These spikes show the existence of long-lived collective modes in the sample. The lifetime of a mode is proportional to the width of the peak in $\mathrm{Im}(D)$. The lowest frequency mode at 1.1 meV is caused by a superposition of the peaks of the four nearly degenerate plasmons. It is superimposed onto the single-particle continuum ranging from 0 to around 2.0 meV. The figure clearly shows that the plasmon peak at 1.1 meV is only weakly Landau damped. The higher-frequency spikes, which correspond to simple single plasmon modes, are associated with poles of the inverse dielectric response function lying just off the real frequency axis. They have the usual Lorentzian line shapes of long-lived quasiparticles. Intraband plasmons in the $1\rightarrow2$ continuum are very weakly damped because of the small wavefunction overlap between the first and second subbands localized at opposite interfaces. Only modes lying inside the electron-hole continua are seen here. Plasmons outside the single-particle regions have infinite lifetime within the RPA approximation and do not appear in $\mathrm{Im}(D)$. Thus, to obtain the full picture of the plasmon dispersion of our sample, we combine the results from (1) finding the zero's of the determinant of the dielectric function and (2) the spikes in the imaginary part of the density-density correlation function. For comparison, Fig. 8(a) shows the imaginary part of D_0, the density-density correlation function in the absence of Coulomb interaction. This function represents, therefore, the single-particle excitation spectra.

We find three groups of intraband plasmon modes.

(1) A group of plasmon modes, labeled "1,2,3,4,5," at high energies. For these modes all charges within each well move in phase (corresponding to the $\nu=1$ plasmon in the single-well model above). We have shown that in this case the Coulomb fields outside the wells are strong. Therefore the interwell Coulomb interaction for these modes is strong and leads to strong splitting of the coupled plasmon modes (modes $n=1,2,3,4,5$). These modes are analogous to those obtained by Fasol *et al.*[9] using a much simpler model.[4] Mode 5 is not observed in the present sample. We did observe a corresponding mode in a different sample structure, but its intensity was extremely weak under the conditions of measurement.

(2) A group Q of plasmon modes at intermediate energies and showing intermediate splitting due to the interlayer Coulomb interaction in the calculation. The charge density associated with these modes corresponds to the $\nu=2$ plasmon mode in the single-well model above.

(3) A group O of plasmon modes at lowest energy. For this group of modes the charge density oscillations within each well are thus that the fields outside the wells extremely small (similar to mode $\nu=3$ in the single-well case). As the Coulomb fields outside the wells are very small, the coupling between the wells is also very small. Consequently, Fig. 5(a) shows no splitting and this mode is fourfold degenerate. This degeneracy explains the very strong Raman scattering strength at this mode.

Mode S is the $3\rightarrow4$ intersubband plasmon. This mode is seen in our measurements, and it is well reproduced by

the calculation, since we are using the *full* polarization propagator. Our calculated split-off mode P is an intrasubband plasmon mode presumably due to the first well which we have taken to have only two filled subbands. In isolation these two subbands would support a symmetric and an antisymmetric plasmon branch. Once coupled with the other four wells, the symmetric branch becomes part of the band of modes 1 to 5. The asymmetric mode couples only weakly and is seen as mode P. An alternative explanation would be that P is due to a lower carrier concentration in the top well due to some surface depletion. Figure 5(a) thus shows that our calculation and the above explanations describe the measured plasmon dispersion of our sample satisfactorily.

It must be pointed out that in order to obtain quantitative agreement between theory and experiment for modes O and Q it is essential to use the full RPA form for the two-dimensional electron-gas polarizability, as we have done here, rather than the long-wavelength high-frequency form for the polarization propagator. The reason for this is that modes O and Q lie close to the intrasubband electron-hole continua where the simple high-frequency form for the two-dimensional electron-gas polarizability is no longer valid.

V. COMPARISON WITH PREVIOUS WORK

It is appropriate at this point to place the present results and interpretations in context of previous work. The first report of intrasubband plasmons in modulation-doped multiple-quantum wells is by Olego *et al.*[7] The sample of Ref. 7 has a sufficiently large number of wells that $q_\perp$ is conserved during the light scattering, and in addition the coupled plasmon modes lie very close together. Thus, the Raman signal consists of a few close-lying coupled plasmon mode lines, which are not resolved. In Ref. 8 a sample with a smaller number of layers ($N=15$) is used: $q_\perp$ conservation still applies approximately. Thus, the Raman scattering still selects a few plasmon lines, but the splitting between them could be observed.

An initial part of the work was reported previously.[9] In Ref. 9 we studied a single five-well sample, and we concluded from Shubnikov–de Haas and from Hall measurements that only a single subband per well was occupied. We obtained the coupled-layer plasmon spectra. We reported observation of single-particle excitation spectra, and we demonstrated the sharply peaked shape of the single-particle spectra, characteristic for two-dimensional electrons. We interpreted the measured plasmon dispersion using a simple model, assuming a single infinitely thin sheet of electrons in each well.[4] Using these approximations we obtained reasonable explanation for the coupled plasmon spectra as well as for the single-particle excitation spectra.

The present work shows, that in our specific quantum wells, three subbands are occupied. The discrepancy seems to arise from the fact that Hall, Shubnikov–de Haas, and single-particle Raman measurements seem to be much less sensitive to the electrons at the "inverted interface," which has much lower mobility, and second, from the fact that the third subband only shows very low occupation. Thus our work shows that a very thorough study is necessary to establish a complete characterization of the subband population—particularly to determine the carrier concentration at the "inverted," low mobility, interface. Comparing the plasmon dispersion in Fig. 2 of Ref. 9 with the present results [Fig. 5(a)] shows that we now understand several features in Ref. 9. Thus the very strong plasmon peak O, which was not understood in Ref. 9, corresponds to those plasmon modes, where the carriers within each well oscillate such that the fields outside the wells vanish. The splitting of modes B and C in Ref. 9 can be understood as the mixing of intersubband and intrasubband plasmon No. 5. The present paper shows that mode C of Ref. 9 is now attributed to the coupled plasmon mode 5 with some admixture of the $3\rightarrow4$ intersubband transition. The mixing of the intrasubband plasmons with the $3\rightarrow4$ intersubband transition is shown in the calculated results in Fig. 5(a) of the present paper. We also see that Jain and Allen's model[4] of a single infinitely thin sheets of electrons would be expected to give a reasonable description of the highest-energy plasmon mode [mode (a) in Fig. 6 of the present paper], where all electrons in each well oscillate in phase. Thus the present paper demonstrates how the details of the subband population are reflected in the intrasubband plasmon dispersion.

VI. CONCLUSION

In conclusion, we have measured with Raman scattering the dispersion of the plasmon modes of a multiple-quantum-well structure with $N=5$ wells and $M=3$ filled subbands per well. To explain the experimental plasmon dispersion we have calculated the full inverse dielectric function in the RPA. We argue that the long-wavelength high-frequency limit is not adequate in the present case. We determine the subband structure experimentally and calculate the wave function using self-consistent band-structure calculations. We calculate the plasmon dispersion and the single-particle excitation spectra using the subband structure and the calculated wave functions.

We show that in this sample with $N=5$ wells and $M=3$ filled subbands per well ($M=2$ subbands in the case of the first well), the dispersion of the intrasubband plasmon modes consists of M groups of modes. The separation of these M groups is due to the strong intrawell interaction of the carriers in different subbands within the same well. Each of these M groups of modes corresponds to a particular plasmon eigenmode of a single isolated well. For the highest group of modes all charges inside each well move in phase. The interlayer Coulomb interaction splits each of these M groups of modes into N plasmon eigenmodes. This splitting differs strongly for different types of modes according to the magnitude of the electric field outside the well. We identify the different modes by comparing *full* RPA calculations ("full" means that we do not use the common high-frequency, long-wavelength approximation) of the inverse

dielectric function with Raman measurements. We investigate the Landau damping. We find Raman spectra from "acoustic" plasmons in regions, where intrasubband Landau damping occurs.

Thus we find a hierarchy of splittings in the plasmon dispersion: a strong splitting into various groups of modes due to the strong intrawell interaction and a weaker splitting of the modes within these groups due to the weaker interwell Coulomb interaction. Thus Raman measurements of the plasmon dispersion together with calculations enable us both to test the calculational methods and, second, we show that these Raman measurements also are a method to analyze the electron distribution in modulation-doped quantum-well samples.

ACKNOWLEDGMENTS

We gratefully acknowledge helpful discussions and support of this work by M. Cardona. We are grateful to H. Hirt, M. Siemers, and P. Wurster for their expert technical assistance with the experiments, which were performed at the Max-Planck-Institute in Stuttgart. R.D.K.-S. expresses his gratitude to J. C. Inkson for support of this work at Exeter University.

---

*Present address: Department of Physics, Uppsala University, S-75121 Uppsala, Sweden.

†Present address: Department of Physics, University of Michigan, Ann Arbor, MI 48109.

[1]H. Daembkes and G. Weimann, Appl. Phys. Lett. **52**, 1404 (1988).

[2]S. Das Sarma and J. J. Quinn, Phys. Rev. B **25**, 7603 (1982).

[3]A. C. Tselis and J. J. Quinn, Phys. Rev. B **29**, 3318 (1984).

[4]J. K. Jain and P. B. Allen, Phys. Rev. Lett. **54**, 2437 (1985).

[5]R. D. King-Smith and J. C. Inkson, Phys. Rev. B **33**, 5489 (1986).

[6]G. Eliasson, P. Hawrylak, and J. J. Quinn, Phys. Rev. B **35**, 5569 (1987).

[7]D. Olego, A. Pinczuk, A. C. Gossard, and W. Wiegmann, Phys. Rev. B **26**, 7867 (1982).

[8]A. Pinczuk, M. G. Lamont, and A. C. Gossard, Phys. Rev. Lett. **56**, 2092 (1986).

[9]G. Fasol, N. Mestres, H. P. Hughes, A. Fischer, and K. Ploog, Phys. Rev. Lett. **56**, 2517 (1986).

[10]V. Z. Kresin and H. Morawitz, Phys. Rev. B **37**, 7854 (1988).

[11]F. Stern, Phys. Rev. Lett. **18**, 546 (1967).

[12]S. Das Sarma and A. Madhukar, Phys. Rev. B **23**, 805 (1981).

[13]S. Das Sarma, Phys. Rev. B **29**, 2334 (1984).

[14]G. Fasol, N. Mestres, M. Dobers, A. Fischer, and K. Ploog, Phys. Rev. B **36**, 1565 (1987).

[15]T. Ando, A. B. Fowler, and F. Stern, Rev. Mod. Phys. **54**, 473 (1987).

[16]U. Ekenberg (unpublished).

[17]T. Ando, J. Phys. Soc. Jpn. **51**, 3893 (1982).

[18]J. Menéndez, A. Pinczuk, D. J. Werder, A. C. Gossard, and J. H. English, Phys. Rev. B **33**, 8863 (1986).

[19]M. Altarelli, Phys. Rev. B **28**, 842 (1983).

[20]N. Tzoar and C. Zhang, Phys. Rev. B **34**, 1050 (1986).